

Article

Synthesis and Physical Properties of NbMnP Single Crystals

Jianda Zhao ¹, Zhixue Shu ¹, Ranuri S. Dissanayaka Mudiyansele ² , Weiwei Xie ² and Tai Kong ^{1,3,*}

¹ Department of Physics, University of Arizona, Tucson, AZ 85721, USA; jdzhao@email.arizona.edu (J.Z.); zhixueshu@email.arizona.edu (Z.S.)

² Department of Chemistry and Chemical Biology, Rutgers University, Piscataway, NJ 08854, USA; rsd96@chem.rutgers.edu (R.S.D.M.); wx101@chem.rutgers.edu (W.X.)

³ Department of Chemistry and Biochemistry, University of Arizona, Tucson, AZ 85721, USA

* Correspondence: tkong@arizona.edu

Abstract: Single crystalline NbMnP was grown by the high-temperature solution growth technique and characterized by room temperature X-ray diffraction, temperature- and field-dependent magnetization, temperature-dependent resistivity, and heat capacity measurements. NbMnP is isostructural to TiNiSi with the space group of Pnma. Physical characterizations suggest that NbMnP is metallic and goes through an anti-ferromagnet transition at around 230 K with a weak magnetic anisotropy. A small ferromagnetic component is found to be perpendicular to [010].

Keywords: magnetism; single crystal; antiferromagnet



Citation: Zhao, J.; Shu, Z.; Mudiyansele, R.S.D.; Xie, W.; Kong, T. Synthesis and Physical Properties of NbMnP Single Crystals. *Magnetism* **2022**, *2*, 179–185. <https://doi.org/10.3390/magnetism2020013>

Academic Editor: Lukasz Hawelek

Received: 4 May 2022

Accepted: 2 June 2022

Published: 7 June 2022

Publisher's Note: MDPI stays neutral with regard to jurisdictional claims in published maps and institutional affiliations.



Copyright: © 2022 by the authors. Licensee MDPI, Basel, Switzerland. This article is an open access article distributed under the terms and conditions of the Creative Commons Attribution (CC BY) license (<https://creativecommons.org/licenses/by/4.0/>).

1. Introduction

Understanding magnetism in different crystalline and chemical environments has been one of the main drives for condensed matter physics [1–3]. Part of this pursuit is to characterize the magnetic properties of different materials, particularly a chemically tunable family of compounds where the Fermi level can be tuned to realize different ground states [4]. One of the such large family of compounds can be found in the TiSiNi structure type [5]. Various interesting physical states were reported, such as ferromagnetism in ZrMnP and HfMnP [6], antiferromagnetism in TbMnSi [7], and superconductivity in ZrRuP [8]. Although many compounds were chemically discovered in this family, detailed magnetization has not been fully studied.

The magnetic characterization of NbMnP was only conducted very recently via bulk magnetization and neutron scattering measurements. A non-collinear spin structure was identified with the Dzyaloshinskii–Moriya (DM) interaction, speculated to contribute to a weak ferromagnetic component in the spin structure. However, due to a lack of anisotropic magnetization characterization, such a DM contribution was not clear [9]. In this study, a single crystalline NbMnP was synthesized and characterized, which provides evidence that favors the spin structure model that requires a DM interaction.

2. Experimental Methods

NbMnP single crystals were grown via a high temperature solution growth technique [10]. Manganese powder (Alfa Aesar, 99.6%), niobium powder (Alfa Aesar, 99.8%), and phosphorus lump (Beantown Chemical, 99.999%) were packed in the Canfield Crucible Set [11] with a molar ratio of Mn:Nb:P = 82.65:1.67:12.35, and sealed in a silica ampoule under vacuum. The ampoule was then heated up to 1200 °C over 5 h, dwelled there for 12 h, and slowly cooled down to 1000 °C over 120 h for decanting. Air stable NbMnP crystals grew in a blade shape (Figure 1 inset), similar to ZrMnP and HfMnP [6]. Due to the similarity in crystal structure and morphology, the crystalline orientation of NbMnP was determined following the guideline for ZrMnP, indicating that the long axis of the blade crystal is [010].

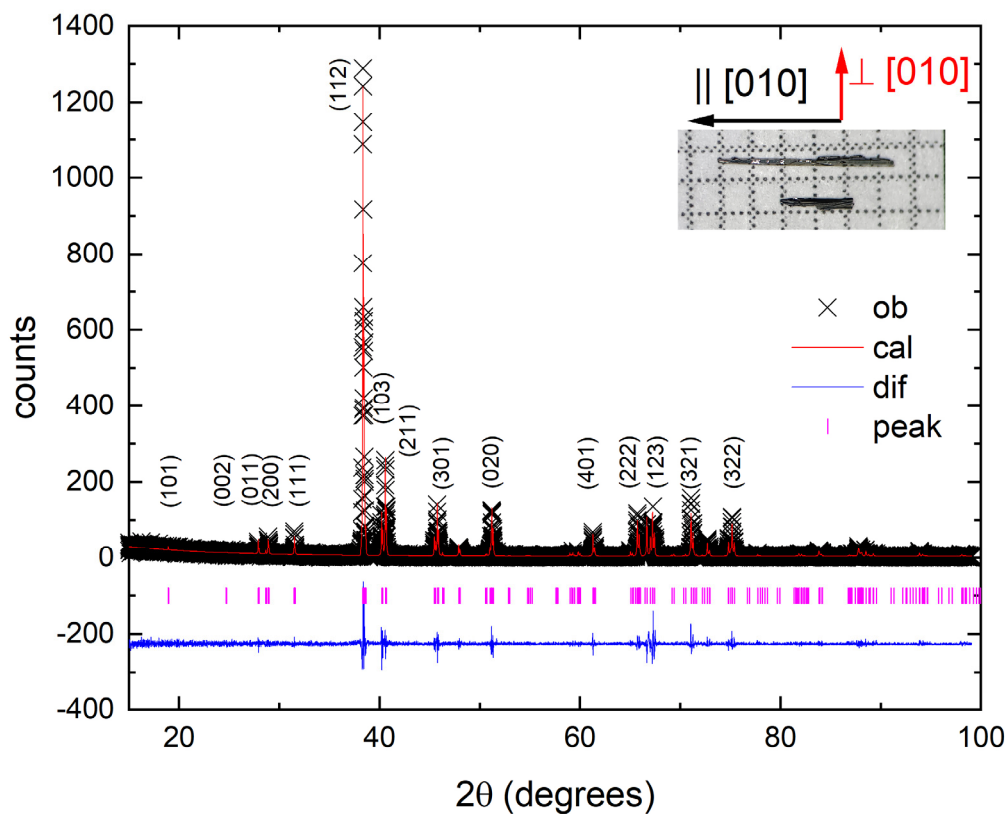


Figure 1. Powder X-ray diffraction result for NbMnP. Observed diffraction data are shown as black crosses. Calculated pattern is shown by the red solid line. The difference between observed and calculated result is shown in blue. Diffraction peak positions are shown by magenta ticks. Major diffraction peaks are indexed. Inset shows as-grown NbMnP single crystals on a millimeter grid paper. Crystalline orientation is determined based on the crystalline morphology.

Room temperature powder X-ray diffraction (PXRD) was measured by using a Bruker D8 Discover diffractometer, with a microfocus and Cu K α radiation ($\lambda = 1.5406 \text{ \AA}$). A collection of NbMnP single crystals were ground into powder and spread evenly on vacuum greased VWR micro cover glass. Powder X-ray refinement was conducted using GSAS using the Le Bail method [12,13]. The room temperature crystal structure was determined using a Bruker D8 Quest Eco single crystal X-ray diffractometer (SXR), equipped with Mo radiation ($\lambda_{K\alpha} = 0.71073 \text{ \AA}$) and a Phonon II detector. The data were collected with an ω of 0.5° per scan and an exposure time of 10 s per frame. A SHELXTL package with the direct methods and full-matrix least-squares on the F^2 model were used to obtain the structural solutions for NbMnP.

Physical properties were measured using a Quantum Design physical property measurement system (PPMS) Dynacool. Anisotropic magnetization was measured using the vibrating sample magnetometer (VSM) option. A collection of single crystals was aligned and glued to a silica sample holder with GE varnish to distinguish between $H \parallel [010]$ and $H \perp [010]$. Temperature-dependent resistance of NbMnP was measured by using four-probe technique. Platinum wires were attached to samples along the [010] direction using DuPont 4929 N silver paint. Temperature-dependent heat capacity was measured using a two-tau relaxation method.

3. Results and Discussion

The crystal structure of NbMnP was confirmed by both PXRD and SXR. The room temperature PXRD data for NbMnP is shown in Figure 1. All peaks can be indexed with an orthorhombic crystal structure in the space group $Pnma$, isostructural to TiNiSi,

which indicates a good sample quality of the single crystals. The atomic position and cell parameters were further refined using room temperature SXRD. Detailed refinement results and structural parameters are shown in Tables 1 and 2. In general, the crystal structure is consistent with previously reported results [9,14].

Table 1. Single crystal refinement and structural parameters for NbMnP.

Empirical Formula	NbMnP
Formula weight	178.82
Temperature	299 (2) K
Wavelength	0.71073 Å
Crystal system, space group	Orthorhombic, Pnma
Unit cell dimensions	a = 6.184 (7) Å b = 3.560 (4) Å c = 7.217 (9) Å
Volume	158.9 (3) Å ³
Z, Calculated density	4
Absorption coefficient	15.508
F (000)	324
Crystal size	~20 μm × 20 μm × 20 μm
θ range (°)	4.340 to 34.946
Limiting indices	h = −9 to 7 k = −5 to 5 l = −9 to 9
Reflection collected	2316
Independent reflections	393
Completeness to θ = 25.242°	100
Absorption correction	None
Refinement method	Full-matrix least-squares on F ²
Data/restraints/parameters	393/0/20
Goodness-of-fit on F ²	1.173
Final R indices [I > 2σ (I)]	R1 = 0.0365, wR2 = 0.0577
R indices (all data)	R1 = 0.0460, wR2 = 0.0598
Extinction coefficient	0.042 (3)
Largest diff. peak and hole	1.735 and −2.419 e. Å ^{−3}

Table 2. Atomic coordinates and equivalent isotropic displacement parameters of NbMnP at 299 (2) K. (U_{eq} is defined as one-third of the trace of the orthogonalized U_{ij} tensor (Å²)).

Atom	Wyckoff.	Occ.	x	y	z	U_{eq}
Nb1	4c	1	0.03093 (9)	$\frac{1}{4}$	0.67220 (9)	0.0048 (2)
Mn2	4c	1	0.14117 (15)	$\frac{1}{4}$	0.05925 (15)	0.0034 (2)
P3	4c	1	0.2676 (3)	$\frac{1}{4}$	0.3695 (2)	0.0041 (3)

Anisotropic magnetization data of NbMnP are shown in Figure 2. As all single crystals have a blade-shaped morphology, the crystalline orientation can be distinguished between the magnetic field applied along the blades ($H \parallel [010]$) and that is perpendicular to the blades ($H \perp [010]$). Above 250 K, the magnetization is nearly isotropic and follows a Curie–Weiss paramagnetic behavior. A Curie–Weiss fit ($M/H = C/(T - \theta_{cw})$, where C is the Curie constant and θ_{cw} is the Curie–Weiss temperature, to the magnetization data around 300 K yields an effective moment $\mu_{eff} \sim 2.5 \mu_B/\text{Mn}$ and a Curie–Weiss temperature of $\theta_{cw} \sim 15$ K. Fit curves are shown by the dashed lines in Figure 2. Compared to the recent report on ferromagnetic ZrMnP and HfMnP [6], where the Mn saturation moment is around $2 \mu_B$, the Mn magnetic moment in NbMnP is comparable in size. However, recent neutron scattering suggests a much smaller itinerant Mn moment of $1.2 \mu_B$. Assuming the Mn

moment is temperature-independent, a higher temperature magnetization measurement may be helpful to better determine the paramagnetic behavior in NbMnP [9].

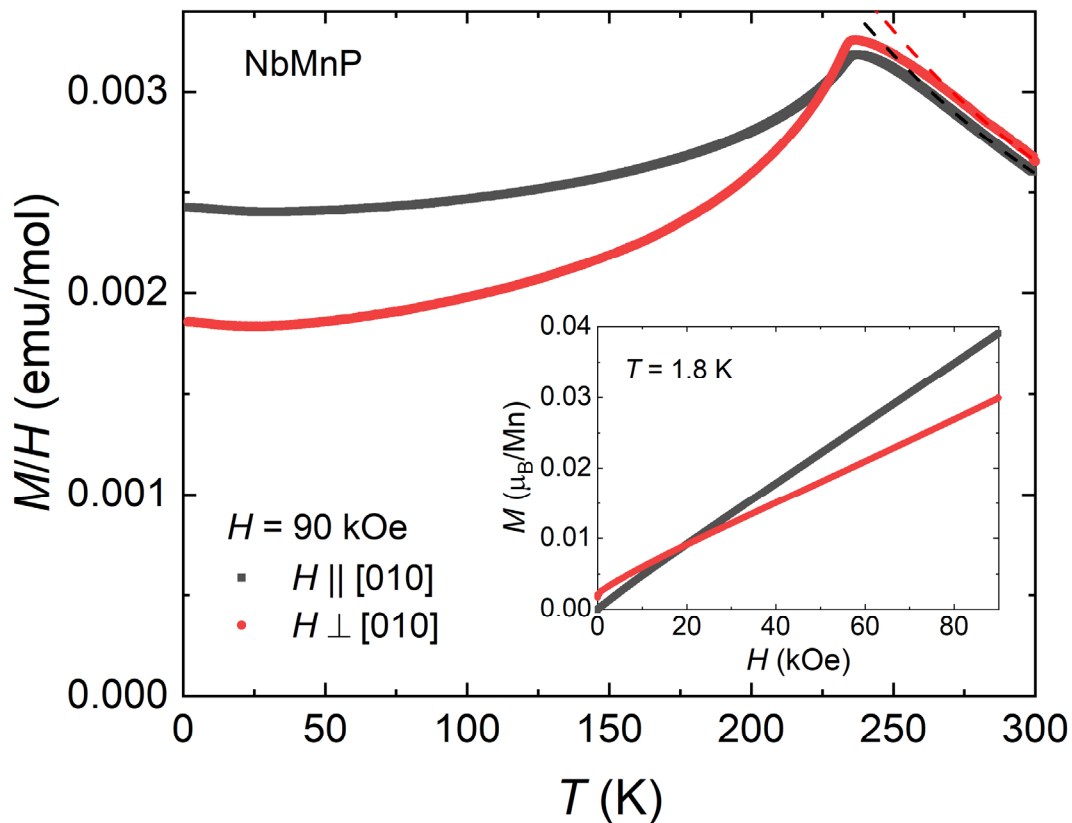


Figure 2. Temperature-dependent anisotropic magnetization of NbMnP measured at 90 kOe. Dashed lines represent paramagnetic Curie–Weiss fit. Inset shows anisotropic isothermal magnetization measured at 1.8 K.

As the temperature decreases, a clear cusp can be observed in the magnetization, consistent with an antiferromagnetic transition. A weak magnetic anisotropy is developed in the magnetically ordered state at a low temperature, with $H \parallel [010]$ yielding a larger magnetization. This is consistent with the reported easy plane magnetic anisotropy that has magnetic moments perpendicular to the b -axis [9]. Although not shown in this paper, a small upturn in magnetization can be observed at the phase transition temperature when a much smaller magnetic field is applied, similar to data shown in Ref. [9]. Such an upturn can be attributed to a very weak ferromagnetic component. The inset of Figure 2 shows the isothermal magnetization measured at 1.8 K. No metamagnetic transition was observed up to 90 kOe. A small ferromagnetic component can be observed for $H \perp [010]$, but not for $H \parallel [010]$. This observation favors the model that predicts a ferromagnetic component along the a -axis rather than the b -axis, which implies that an additional DM interaction needs to be considered to understand the magnetic structure of NbMnP [9]. Due to sample geometry limitations, a more detailed magnetic anisotropy between the a - and c -axis was not determined in this study.

The temperature-dependent resistivity of NbMnP is shown in Figure 3. It shows a typical metallic behavior. A clear kink can be observed at the magnetic phase transition, consistent with a loss of spin disorder scattering upon long-range magnetic ordering [15]. The residual resistance ratio (RRR) is around 2.1, similar to a recent single crystal result which uses the same sample synthesis method [9].

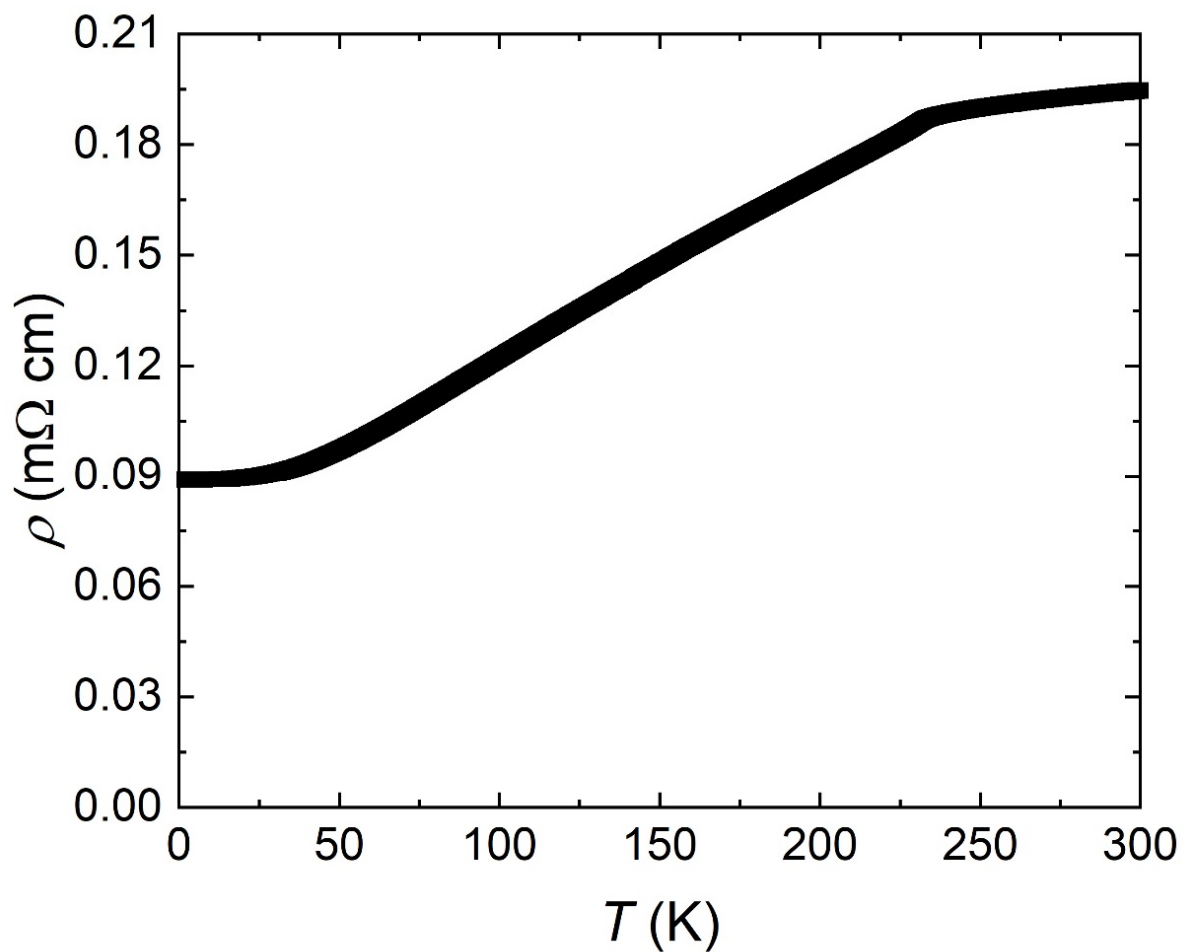


Figure 3. Zero-field temperature dependent resistivity of NbMnP.

Figure 4 shows the temperature-dependent specific heat of NbMnP. At room temperature, the specific heat value is close to the expected Dulong–Petit limit. A clear λ -shaped feature signatures a second-order phase transition at ~ 230 K. The phase transition temperature in specific heat is consistent with the previously shown magnetization and resistivity data. By taking the peak temperature in specific heat, the derivative of resistivity ($d\rho/dT$) [16] and the derivative of magnetic susceptibility times temperature ($d\chi T/dT$) [17], the antiferromagnetic transition temperature of NbMnP can be determined to be 230 ± 3 K. The upper inset of Figure 4 shows the C_p/T vs. T^2 plot. The observed linear trend agrees with expected T^3 dependence of phonon and antiferromagnetic magnon contributions [18]. The electronic-specific heat is found to be 19 mJ/mol K².

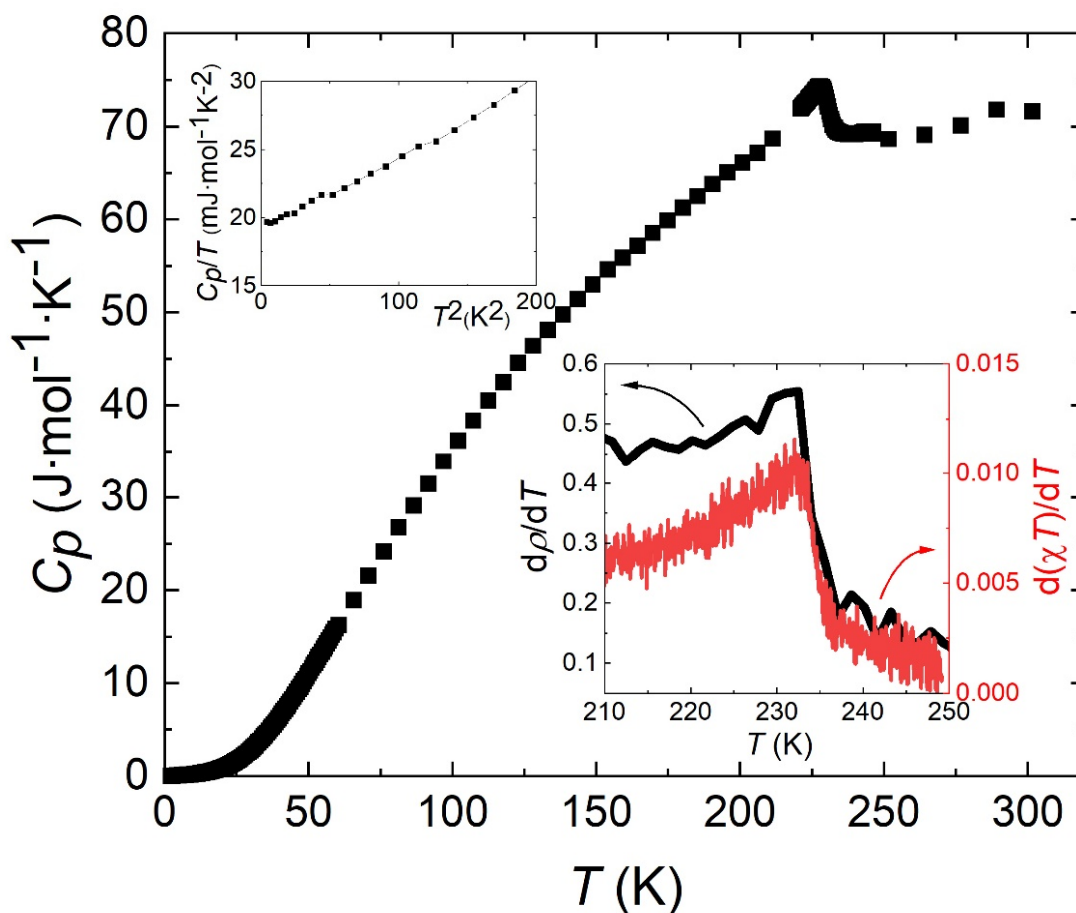


Figure 4. Zero-field temperature-dependent heat capacity of NbMnP. The upper insert shows C_p/T versus T^2 at low temperature. The lower insert shows $d\rho/dT$ and $d(\chi T)/dT$ around magnetic transition temperature.

4. Conclusions

In conclusion, single crystalline NbMnP was obtained using a high temperature solution growth technique. Room temperature X-ray diffraction confirmed that NbMnP crystallizes in an orthorhombic, $Pnma$ space group, which is isostructural to TiNiSi. Temperature-dependent magnetization, resistivity, and heat capacity measurements suggest that NbMnP goes through a second order antiferromagnetic ordering at 230 ± 3 K. Based on low-temperature anisotropic magnetization data, a small ferromagnetic component was found to be perpendicular to $[010]$ direction. This is consistent with a recent neutron scattering result on NbMnP [9]. In the future, more detailed modeling may help reveal the role of a DM interaction in this compound.

Author Contributions: Conceptualization, T.K.; Material synthesis and physical property measurements, J.Z. and Z.S.; Single crystal diffraction, R.S.D.M. and W.X.; Writing, J.Z., R.S.D.M., W.X. and T.K. All authors have read and agreed to the published version of the manuscript.

Funding: This work is supported by the University of Arizona startup funds. Work at Rutgers was supported by the U.S. Department of Energy (DOE), Office of Science, Basic Energy Sciences under award DE-SC0022156.

Data Availability Statement: The data presented in this study are available on request from the corresponding author.

Conflicts of Interest: The authors declare no conflict of interest.

References

1. Anderson, P.W. Localized Magnetic States in Metals. *Phys. Rev.* **1961**, *124*, 41. [[CrossRef](#)]
2. Anderson, P.W. The Resonating Valence Bond State in La₂CuO₄ and Superconductivity. *Science* **1987**, *235*, 1196–1198. [[CrossRef](#)] [[PubMed](#)]
3. Ramirez, A.P. Strongly Geometrically Frustrated Magnets. *Annu. Rev. Mater. Sci.* **1994**, *24*, 453–480. [[CrossRef](#)]
4. Canfield, P.C. New materials physics. *Rep. Prog. Phys.* **2020**, *83*, 016501. [[CrossRef](#)] [[PubMed](#)]
5. Lomnytska, Y.F.; Kuz'ma, Y.B. New phosphides of IVa and Va group metals with TiNiSi-type. *J. Alloys Compd.* **1998**, *269*, 133–137. [[CrossRef](#)]
6. Lamichhane, T.N.; Taufour, V.; Masters, M.W.; Parker, D.S.; Kaluarachchi, U.S.; Thimmaiah, S.; Bud'ko, S.L.; Canfield, P.C. Discovery of ferromagnetism with large magnetic anisotropy in ZrMnP and HfMnP. *Appl. Phys. Lett.* **2016**, *109*, 092402. [[CrossRef](#)]
7. Welter, R.; Venturini, G.; Ijjaali, I.; Malaman, B. Magnetic study of the new TiNiSi-type TbMnSi, DyMnSi and NdMnGe compounds. *J. Magn. Magn. Mater.* **1999**, *205*, 221. [[CrossRef](#)]
8. Müller, R.; Shelton, R.N.; Richardson, J.W.; Jacobson, R.A.J. Superconductivity and crystal structure of a new class of ternary transition metal phosphides TT'P (T ≡ Zr, Nb, Ta and T' ≡ Ru, Rh). *Less-Comm. Met.* **1983**, *92*, 177–183. [[CrossRef](#)]
9. Matsuda, M.; Zhang, D.; Kuwata, Y.; Zhang, Q.; Sakurai, T.; Ohta, H.; Sugawara, H.; Takeda, K.; Hayashi, J.; Kotegawa, H. Noncollinear spin structure with weak ferromagnetism in NbMnP. *Phys. Rev. B* **2021**, *104*, 174413. [[CrossRef](#)]
10. Canfield, P.C.; Fisk, Z. Growth of single crystals from metallic fluxes. *Phil. Mag. B* **1992**, *65*, 1117. [[CrossRef](#)]
11. Canfield, P.C.; Kong, T.; Kaluarachchi, U.S.; Jo, N.H. Use of frit-disc crucibles for routine and exploratory solution growth of single crystalline samples. *Philos. Mag.* **2016**, *96*, 84–92. [[CrossRef](#)]
12. Toby, B.H. EXPGUI, a graphical user interface for GSAS. *J. Appl. Crystallogr.* **2001**, *34*, 210–213. [[CrossRef](#)]
13. Larson, A.C.; Von Dreele, R.B. General Structure Analysis System (GSAS). In *Los Alamos National Laboratory Report LAUR 86-748*; Los Alamos National Laboratory: Los Alamos, NM, USA, 2000.
14. Lomnitskaya, Y.F.; Kondratyuk, G.D.; Zakharets, L.I. Niobium and phosphorus interaction with manganese and copper. *Zh. Neorg. Khim.* **1988**, *33*, 734–737.
15. Kong, T.; Cunningham, C.E.; Taufour, V.; Bud'ko, S.L.; Buffon, M.L.C.; Lin, X.; Emmons, H.; Canfield, P.C. Thermodynamic and transport properties of single crystalline RCo₂Ge₂ (R = Y, La–Nd, Sm–Tm). *J. Magn. Magn. Mater.* **2014**, *358–359*, 212. [[CrossRef](#)]
16. Fisher, M.E.; Langer, J.S. Resistive Anomalies at Magnetic Critical Points. *Phys. Rev. Lett.* **1968**, *20*, 665. [[CrossRef](#)]
17. Fisher, M.E. Relation between the specific heat and susceptibility of an antiferromagnet. *Philos. Mag.* **1962**, *7*, 1731–1743. [[CrossRef](#)]
18. Tari, A. *The Specific Heat of Matter at Low Temperatures*; World Scientific: Singapore, 2003.